An Augmented Catenary Model for Underwater Tethered Robots

Martin Filliung[1, 2], Juliette Drupt[1], Charly Peraud[1],
Claire Dune[1], Nicolas Boizot[2], Andrew Comport[3], Cedric Anthierens[1], Vincent Hugel[1]

I. Introduction

This study focuses on shape estimation of underwater remotely operated vehicle (ROV) tethers to be used in robot control for path following or obstacle avoidance. A fixed-length cable only subject to its own weight can be modeled as a catenary. However, the extension of the catenary model to a moving ROV's tether is not straightforward due to hydrodynamic effects. Assuming no dynamic effects the tether's shape can be estimated from the relative position of the two attachment points and the catenary model such as in [1], [2] and from the local cable tangent orientation [3]. But as soon as the robot velocity increases, underwater drag involves hydrodynamic forces that move the cable from its vertical plane, even at low speed [4].

The main contribution of the present study is the introduction of a new enhanced catenary model that incorporates full tilting of the tether during surge or sway motion of the underwater robot. The relevance of this geometric model is confirmed through experiments conducted on eight cables with different mechanical properties (Fig. 1).

II. Related work

Underwater ROV tether shape can be estimated from the measurements of inertial sensors placed along it [5]. However, these methods require the use of a specially designed cable. In addition, the accuracy of these methods decreases with the cable's length due to error accumulation.

Other strategies make use of physical or geometrical cable models. A physical model can be developed based on the cable's hydrodynamics and the forces acting upon it [6], [7], [8], [9]. Although such models are the most comprehensive and designed to closely match the physics, they are computationally intensive and require an extensive understanding of multiple parameters which are difficult to measure under actual circumstances, such as water current or thruster parameters. As a result, simpler models are often preferred. The cable may be constrained to a simplified geometric shape artificially, for instance by introducing weights or sliding floaters to make it piecewise linear [10], [11], [12]. Some studies employ the catenary model, a hyperbolic curves, for underwater or aerial settings with an adequate cable that conform to the model's hypothesis [13], [3], whereas parabolic curves may also be utilized in aerial scenarios [14].

[1]COSMER Laboratory, Univ. de Toulon, France
[2]Univ. de Toulon, Aix Marseille Univ, CNRS LIS, Marseille, France
[3]CNRS I3S Laboratory, Univ. Côte d'Azur, Sophia Antipolis, France

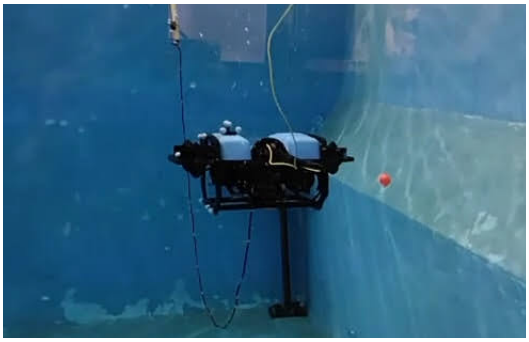

Fig. 1: Experimental setup. A dark red cable connects the ROV to a fixed point. Optical markers are regularly placed on the cable for underwater motion tracking. The slack light yellow tether is used for communications with the ROV.

III. Modeling and estimation

Let $\mathcal{F}_w = (\mathbf{O}_w, \mathbf{x}_w, \mathbf{y}_w, \mathbf{z}_w)$ be a fixed Cartesian reference frame with the $\mathbf{z}_w$-axis vertical and pointing upwards.

A. Standard catenary model

The shape of a homogeneous hanging cable, with fixed length L, only subjected to its weight and buoyancy, is defined by a standard catenary curve (Fig. 2). The catenary lies in a vertical plane $\mathcal{P}_v = (\mathbf{O}_v, \mathbf{x}_v, \mathbf{z}_v)$, associated to the Cartesian frame $\mathcal{F}_v = (\mathbf{O}_v, \mathbf{x}_v, \mathbf{y}_v, \mathbf{z}_v)$ where $\mathbf{O}_v$ is the lowest point of the curve, $\mathbf{x}_v$ is horizontal and $\mathbf{z}_v$ is collinear to $\mathbf{z}_w$. Curve points coordinates $({}^vX, {}^vZ) \in \mathcal{P}_v$ are given by:

$$({}^vX, {}^vZ) \in [{}^vX_i, {}^vX_f] \times \mathbb{R} \text{ such that}$$
$${}^vZ = \frac{\cosh({}^vXC) - 1}{C} \tag{1}$$

where $C \in \mathbb{R}_+^*$ is the catenary parameter, and indexes i and f refer to the curve's endpoints. The left superscript indicates the frame in which a coordinate is given.

B. Augmented catenary model

As soon as the underwater cable is moved fast enough, hydrodynamic forces become non-negligible. The drag forces dampens the movement with an amplitude that is proportional to the square of the speed. This effect is amplified by the added mass when significant accelerations are present [15], [6].

In the steady state case where all points on the cable move at the same velocity, they are subjected to the same drag forces. As a consequence, the resulting uniform acceleration of the cable is tilted, and its intensity is increased depending

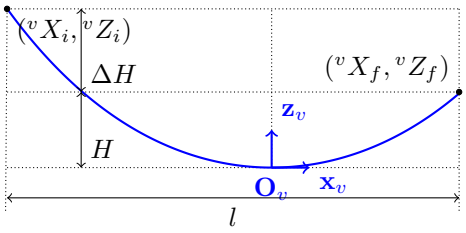

Fig. 2: Catenary curve of length L defined in $\mathcal{P}_v$. Parameters are the sag H, the difference of elevation ΔH and the horizontal distance l between attachment points.

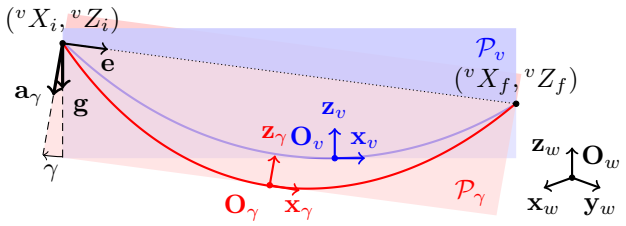

Fig. 3: Standard (blue) and γ-augmented (red) catenary for $\gamma = 10°$.

on the velocity. The addition of two degrees of freedom in the cable shape model to account for this effect is used here to extend the standard catenary model.

The first degree of freedom is a rotation of angle γ around the catenary axis $\mathbf{e}$, which is defined as the unit vector that connects cable endpoints [3] (Fig. 3). This is to consider the deformations of a tether subjected to sway motions, *i.e.* the cable ends move out of the vertical plane, namely $\mathcal{P}_v$. This rotation applied to $\mathcal{F}_v$ and $\mathcal{P}_v$ gives $\mathcal{F}_\gamma = (\mathbf{O}_\gamma, \mathbf{x}_\gamma, \mathbf{y}_\gamma, \mathbf{z}_\gamma)$ and $\mathcal{P}_\gamma$, respectively.

Then, the second degree of freedom, a rotation of angle θ in $\mathcal{P}_\gamma$ (Fig. 4), considers tether deformations caused by surge motions, *i.e.* the two cable ends get closer or further from each other. The approximation of uniform hydrodynamic forces along the cable results in a uniform tilted acceleration $\mathbf{a}_{\theta\gamma}$ with respect to gravity. Let $\mathcal{F}_{\theta\gamma} = (O_{\theta\gamma}, \mathbf{x}_{\theta\gamma}, \mathbf{y}_{\theta\gamma}, \mathbf{z}_{\theta\gamma})$ be the associated Cartesian frame where $\mathbf{z}_{\theta\gamma}$ is parallel to $\mathbf{a}_{\theta\gamma}$ and $\mathbf{y}_{\theta\gamma}$ is parallel to $\mathbf{y}_\gamma$. The two ends of the cable can be expressed in $\mathcal{F}_{\theta\gamma}$ and (1) is used to construct the oriented catenary. This 2-DOF model is named the *$\theta\gamma$-augmented model*.

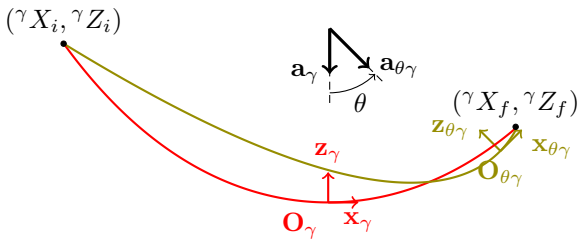

Fig. 4: γ-augmented (red) and $\theta\gamma$-augmented (green) catenary for $\theta = 45°$.

C. Curvilinear discretization and residual

Let us consider $n+1$ 3D measurement points distributed along the cable's length. Accordingly, the model is discretized with respect to the curvilinear abscissa.

Henceforth, the symbols m, v and $\theta\gamma$ are used as indexes referring to the measurements and the estimates of the *standard* and $\theta\gamma$-augmented catenary model variations, respectively. Model points are written:

$$
\begin{aligned}
{}^{w}\mathbf{P}_k^* &= ({}^{w}X_k^*, {}^{w}Y_k^*, {}^{w}Z_k^*) \\
k \in \{0, \dots, n\}, &* \in \{m, v, \theta\gamma\}
\end{aligned}
$$

where indexes $k = 0$ and $k = n$ are the tether endpoints, also indexed i and f. The residual is then written:

$$
\varepsilon_{\mathbf{P}}^* = \frac{1}{n} \sum_{k=0}^{n} \| {}^{w}\mathbf{P}_k^m - {}^{w}\mathbf{P}_k^* \|, \ * \in \{v, \theta\gamma\} \tag{2}
$$

D. Model parameters estimation

1) Catenary parameter: Let L be the tether length, l the horizontal distance and ΔH the difference of elevation between the tether attachment points calculated from the measurements of the initial and final attachment points ${}^{\Diamond}\mathbf{P}_i^m$ and ${}^{\Diamond}\mathbf{P}_f^m$, with $\Diamond \in \{v, \theta\gamma\}$ the frame in which the points are expressed (Fig. 2). The catenary parameter C is estimated by finding the root of function f which relates the curve's length and C [13] (using Brent's method [16]):

$$
f(C) = C^2 \left(L^2 - \Delta H^2\right) - 4 \sinh^2(lC/2)
$$

2) Augmented model parameters: Let $\varepsilon_{\mathbf{P}}^{\theta\gamma}(\theta, \gamma)$ be the residual written as a function of θ and γ (2). Angles θ and γ are estimated by minimizing this function by means of the trust region reflective algorithm [17]:

$$
(\theta, \gamma) = \underset{(\theta,\gamma)\in[-\pi,\pi]^2}{\operatorname{argmin}} \ \varepsilon_{\mathbf{P}}^{\theta\gamma}(\theta, \gamma)
$$

IV. Experiments

The experiment involves a $3\,\mathrm{m}$ weighted seamstress rope as the ROV's mock cable. Its mechanical properties make it an ideal subject for modelization with the catenary model.

The experiment is set up in a $7.2\,\mathrm{m}$ long, $4.2\,\mathrm{m}$ wide and $3\,\mathrm{m}$ deep tank. One end of the cable, namely ${}^{w}\mathbf{P}_n^m$, is attached to a ROV (BlueROV), while the other, namely ${}^{w}\mathbf{P}_0^m$, is fixed and attached to the side of the pool (Fig. 1).

The cable's and robot's positions are recorded by a 5-camera, $100\,\mathrm{Hz}$ *Qualisys*[1] underwater motion capture system. The robot as well as the cable are equipped with passive reflective markers and the cable's markers are evenly spaced out by $0.2\,\mathrm{m}$ ($n = 15$). The calibration of the motion capture system gives a standard deviation of $2.2\,\mathrm{mm}$ across the pool's volume for a known object's length. The points ${}^{w}\mathbf{P}_k^m$ are measured in the *Qualysis* world Cartesian frame which is defined by the positioning of a calibration target that may not be perfectly vertical in the real experiment. This introduces a small offset ($\pm 0.05\,\mathrm{rad}$) for the steady state angles as can be seen in Fig. 6.

[1] See specifications at www.qualisys.com/cameras/underwater

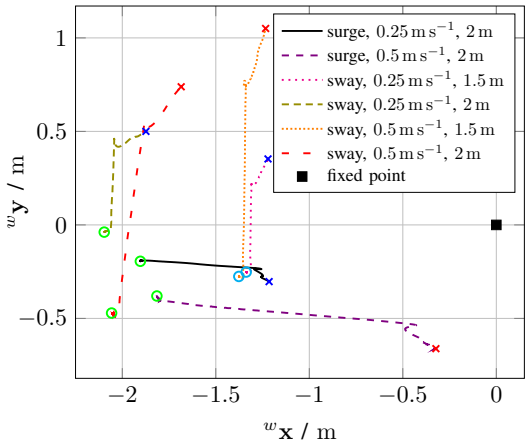

Fig. 5: Top view of the experimental trajectories. Circles refer to initial positions and crosses refer to final positions.

The initial position of the robot is defined such that the robot is stabilized at $1\,\mathrm{m}$ depth and approximately $1\,\mathrm{m}$ from the lateral pool wall facing the fixed attachment point (Fig. 5). Surge and sway movements are conducted individually to investigate the cable's response movement within or without its original vertical plane. The robot repeats the same open-loop control in sway or surge with the same step profile: 1) stabilisation with auto-depth at $1\,\mathrm{m}$ depth for $2\,\mathrm{s}$, 2) abrupt start with constant surge or sway command applied for $2.5\,\mathrm{s}$, 3) reversing of the thrusters for $0.3\,\mathrm{s}$ with a doubled velocity of opposite direction, to obtain an abrupt stop, 4) slow down the thruster for half the initial velocity during $0.2\,\mathrm{s}$ and 5) deactivation of the auto-depth control and complete stop of the thrusters after $13\,\mathrm{s}$. The robot then drifts slowly.

The experiment is repeated three times, under six experimental conditions, which makes it possible to test the reactions of the cable with accelerations of different amplitudes. Each experimental condition is a combination of a direction of motion (sway or surge), a speed ($0.3\,\mathrm{m\,s^{-1}}$ or $0.6\,\mathrm{m\,s^{-1}}$) and a starting point characterized by its horizontal distance from the fixation point (about $1.5\,\mathrm{m}$ or $2\,\mathrm{m}$).

Fig. 6 shows the model variants residuals, angles θ and γ, as well as the robot's speed. These figures show in detail the different phases of the movement: an initial stable position (hydrostatic equilibrium phase), an abrupt start (dynamic phase), a phase of continuous application of a constant command (steady state phase), an abrupt stop (dynamic phase) and a subsequent hydrostatic phase.

A clear correlation appears between the robot's dynamics and the angle γ for sway motion. The estimated γ angle consistently increases with speed during sway movements, whereas θ remains close to zero (Fig. 6a). For surge motion both angles increase with velocity, with θ being greater than the one observed for sway movement (Fig. 6b). However, since γ is larger than expected, let us examine the trajectory displayed in Fig. 5 relative to surge motion with $0.6\,\mathrm{m\,s^{-1}}$ and $2\,\mathrm{m}$. While the primary motion is surge, the trajectory of the robot is not precisely aligned with the fixed point causing

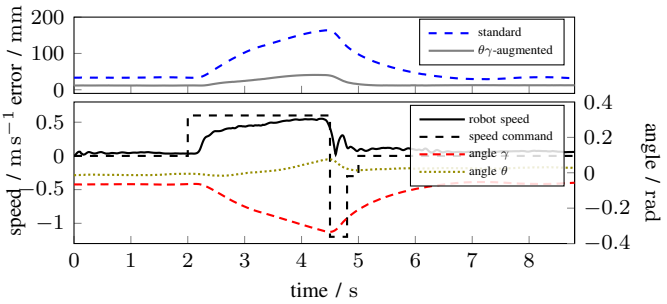

(a) sway motion.

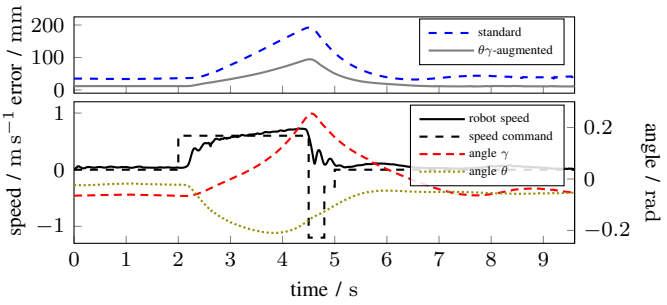

(b) surge motion.

Fig. 6: Model residuals, robot speed and θ, γ angles over time. Speed command of $0.6\,\mathrm{m\,s^{-1}}$ and $2\,\mathrm{m}$ distance.

the cable to move laterally. Although this effect is present throughout all sequences, it is particularly pronounced in this trajectory which explains the values for γ. This demonstrates that our $\theta\gamma$-augmented model is capable of simultaneously managing significant sway and surge movements.

V. Conclusion

This work introduced an augmented catenary model that accounts for the hydrodynamic effects on the tether when the ROV performs surge and sway motion. It incorporates the models presented in the state of the art, which can be found by zeroing one or both of the angles proposed as augmentation parameters.

The results drawn from the experiments carried out on the chosen cable show that the augmented model provides a better estimate of the shape during dynamic phases, compared with the standard catenary model. The accuracy of the model for the cable relies on its relatively high weight and flexibility, as such their measured shape features greater planarity and homogenous tilting of their support plane during motion.

In light of these results, the augmented catenary model will be used in model-based controllers to estimate cable shape and its lowest position for deployment scenarios of tethered robots.

VI. Acknowledgment

This work is funded by the French Research Ministry, the CARTT de l'Université de Toulon.

REFERENCES

[1] D. S. D'Antonio, G. A. Cardona, and D. Saldaña, "The catenary robot: Design and control of a cable propelled by two quadrotors," *IEEE Rob. and Autom. Lett.*, vol. 6, no. 2, pp. 3857–3863, 2021.

[2] D. S. D'Antonio and D. Saldana, "Folding knots using a team of aerial robots," in *IEEE/RSJ Int. Conf. on Intelligent Rob. and Sys.*, Oct. 2022.

[3] J. Drupt, C. Dune, A. I. Comport, S. Sellier, and V. Hugel, "Inertial-Measurement-Based Catenary Shape Estimation of Underwater Cables for Tethered Robots," in *IEEE/RSJ Int. Conf. on Intelligent Rob. and Sys.*, Kyoto, Japan, Oct. 2022.

[4] J. Drupt, C. Dune, A. I. Comport, and V. Hugel, "Validity of the catenary model for moving submarine cables with negative buoyancy," in *3rd IEEE IROS Workshop ROMADO-SI*, Kyoto, Japan, 2022.

[5] J. Frank, R. Geiger, D. R. Kraige, and A. Murali, "Smart tether system for underwater navigation and cable shape measurement," 2013, uS Patent 8,437,979.

[6] N. O.A. and I. Schjølberg, "Finite element cable-model for remotely operated vehicles (rovs) by application of beam theory," *Ocean Eng.*, vol. 163, pp. 322–336, 2018.

[7] Y. Meng, X. Xu, and M. Zhao, "Dynamics calculation of complex deep-sea cable system based on hybrid optimization algorithm," *Ocean Eng.*, vol. 200, p. 107041, 2020.

[8] S. Soylu, B. Buckham, and R. Podhorodeski, "Dynamics and control of tethered underwater-manipulator systems," in *Oceans*. Seattle, WA, USA: MTS/IEEE, 2010, pp. 1–8.

[9] S. Hong, K. Ha, and J. Kim, "Dynamics modeling and motion simulation of usv/uuv with linked underwater cable," *J. of Marine Science and Engineering*, vol. 8, no. 5, 2020.

[10] C. Viel, "Self-management of the umbilical of a rov for underwater exploration," *Ocean Eng.*, vol. 248, p. 110695, Mar. 2022.

[11] ——, "Self-management of ROV umbilical using sliding buoys and stop," *IEEE Rob. and Autom. Lett.*, vol. 7, no. 3, pp. 8061–8068, July 2022.

[12] C. Viel, J. Drupt, C. Dune, and V. Hugel, "ROV localization based on umbilical angle measurement," *Ocean Eng.*, vol. 269, p. 113570, Feb. 2023.

[13] M. Laranjeira, C. Dune, and V. Hugel, "Catenary-based visual servoing for tether shape control between underwater vehicles," *Ocean Eng.*, vol. 200, p. 107018, 2020.

[14] L. Smolentsev, A. Krupa, and F. Chaumette, "Shape visual servoing of a tether cable from parabolic features," in *IEEE Int. Conf on Rob. and Autom.*, London, United Kingdom, May 2023.

[15] T. Fossen, *Handbook of Marine Craft Hydrodynamics and Motion Control*, 05 2011.

[16] R. P. Brent, *Algorithms for minimization without derivatives*. Courier Corporation, 2013.

[17] M. A. Branch, T. F. Coleman, and Y. Li, "A subspace, interior, and conjugate gradient method for large-scale bound-constrained minimization problems," *SIAM Journal on Scientific Computing*, vol. 21, no. 1, pp. 1–23, 1999.